applied sciences

MDPI

Article

Radiotherapy-Induced Lung Cancer Risk in Breast Cancer Patients: A Retrospective Comparison of Hypofractionated and Standard Fractionated 3D-CRT Treatments

Alessia D'Anna [1,2,*], Giuseppe Stella [1,*], Elisa Bonanno [3], Giuseppina Rita Borzì [3], Nina Cavalli [3], Andrea Girlando [4], Anna Maria Gueli [1,2], Martina Pace [3], Lucia Zirone [3] and Carmelo Marino [3]

[1] Department of Physics and Astronomy "E. Majorana", University of Catania, 95123 Catania, CT, Italy
[2] Centro Siciliano di Fisica Nucleare e Struttura della Materia (CSFNSM), 95125 Catania, CT, Italy
[3] Medical Physics Department, Humanitas Istituto Clinico Catanese, 95045 Misterbianco, CT, Italy; carmelo.marino@humanitascatania.it (C.M.)
[4] Radiotherapy Department, Humanitas Istituto Clinico Catanese, 95045 Misterbianco, CT, Italy
* Correspondence: alessia.danna@phd.unict.it (A.D.); giuseppe.stella@dfa.unict.it (G.S.)

Featured Application

This study highlights the potential of Hypofractionated 3D Conformal Radiotherapy (HF 3D-CRT) to reduce the long-term risk of radiation-induced lung cancer compared to standard fractionation (SF 3D-CRT) in early-stage breast cancer patients. These findings support the adoption of HF schedules not only for their clinical convenience but also for their potential benefit in minimizing second cancer risk, reinforcing their role in evidence-based treatment planning.

Abstract

Breast-conserving surgery followed by external beam Radiotherapy (RT) is a standard approach for early-stage Breast Cancer (BC). This retrospective study aims to determine the risk of RT-induced lung cancer for both standard and hypofractionated treatments. Fifty-eight Sicilian women treated at Humanitas Istituto Clinico Catanese (Misterbianco, Italy) between 2015 and 2021 with standard fractionated 3D-CRT (50 Gy in 2 Gy/fraction) were included. All treatment plans were designed using a hypofractionated schedule (42.56 Gy in 2.66 Gy/fraction). An Eclipse™ plug-in script was developed using the Eclipse Scripting Application Programming Interface (ESAPI) to extract patient and treatment data from the Treatment Planning System and compute Organ At Risk (OAR) volume, Organ Equivalent Dose (OED), Excess Absolute Risk (EAR), and Lifetime Attributable Risk (LAR) using the Schneider Mechanistic Model and reference data from regional populations, A-bomb survivors, and patients with Hodgkin's Disease (HD). The OED distributions exhibited a statistically significant shift toward higher values in standard fractionated plans ($p < 0.01$, one-tailed paired Student's t-test), leading to increased EAR and LAR. These results indicate that hypofractionated treatment may lower the risk of radiation-induced lung cancer. The feasibility of a priori risk estimation was evaluated by integrating the script into the TPS, allowing rapid comparison of SF and HF plans during planning.

Keywords: Eclipse™ scripting; secondary induced cancer; organ equivalent dose; excess absolute risk; lifetime attributable risk; 3D-CRT; long-term risk

Academic Editor: Giorgio De Nunzio

Received: 13 June 2025
Revised: 22 July 2025
Accepted: 25 July 2025
Published: 29 July 2025

Citation: D'Anna, A.; Stella, G.; Bonanno, E.; Borzì, G.R.; Cavalli, N.; Girlando, A.; Gueli, A.M.; Pace, M.; Zirone, L.; Marino, C. Radiotherapy-Induced Lung Cancer Risk in Breast Cancer Patients: A Retrospective Comparison of Hypofractionated and Standard Fractionated 3D-CRT Treatments. *Appl. Sci.* **2025**, *15*, 8436. https://doi.org/10.3390/app15158436

1. Introduction

Breast Cancer (BC) is the most frequent neoplasm in women. In recent years, the life expectancy of patients with BC has increased due to screening-related earlier detection and treatment improvements. The current gold standard for early-stage BC is conserving surgery followed by external beam radiotherapy (RT). This adjuvant treatment may reduce the incidence of locoregional recurrence and BC deaths [1]. However, RT inevitably exposes structures proximal to the Planning Target Volume (PTV), such as the ipsilateral lung considered in this study. Although the 5-year survival increased to 85% or higher in many countries [2], exposure to ionizing radiation remains a concern. Epidemiological studies have shown correlations between exposure to ionizing radiation and the long-term carcinogenesis risk [3]. This type of risk depends on several factors [4]: attained patient's age, age of the patient at the time of exposure, total dose, dose fractionation schedule, and Organ At Risk (OAR) dose distribution. Therefore, it is important to calculate the specific risk for each patient based on their treatment plan and characteristics rather than generalizing it.

Schneider's mechanistic model [5,6] provides patient-, organ-, and treatment-specific risk estimation starting from biological considerations about cell killing, mutation, and repopulation. This model is based on the Life Span Study (LSS) [3], a comprehensive investigation of data from atomic bomb survivors. The model parameters are derived by aligning this data with epidemiological studies on Hodgkin's Disease (HD) [6–11], as well as using population-specific statistical parameters.

At Humanitas Istituto Clinico Catanese (H-ICC) in Misterbianco (Italy), Breast Cancer Radiotherapy (BC RT) treatments are typically carried out using two distinct fractionation schemes, based on clinical and radiobiological considerations: the Standard Fractionation (SF) approach, which delivers a total dose of 50 Gy in 25 daily fractions, and the Hypofractionation (HF) approach, which deliver a total dose of 42.56 Gy in 16 daily fractions. Evidence from randomized trials and institutional series supports the effectiveness and safety of hypofractionation for the adjuvant treatment of regional lymph nodes [12]. Although hypofractionation is supported by evidence of safety and efficacy in the regional lymph node setting, it is not suitable for all patients. Those with postoperative complications, large breasts, or breast implants may face higher risks of late toxicity and cosmetic effects. This clinical variability justifies the need to investigate and compare both treatment approaches, as performed in the present study.

Secondary tumors do not arise immediately following exposure to ionizing radiation; rather, a latency period exists between treatment and disease onset [13]. Several studies have retrospectively investigated the risk of RT-induced lung cancer in BC patients [14–19]. However, past epidemiological data on cancer induction are not sufficient, because radiation therapy techniques have changed substantially in recent decades [8]. Risk estimation can be performed using models. The Linear No-Threshold (LNT) model, derived from the LSS on A-Bomb survivors, provides a dose–response relationship [3]. While the data support a linear response between 0 and 2 Gy, a flattening of the dose–response curve is observed at higher doses. Therefore, estimating carcinogenesis risk in RT, where higher doses and various fractionation schemes are used, requires a more appropriate dose–risk model. Several approaches have been proposed by the scientific community to address this issue [4]. Gray et al. [20] found that cancer induction results from the interplay between the induction of carcinogenic mutations and radiation-induced cell kill. Starting from this concept, a competition model based on the Linear Quadratic (LQ) model was included in the UNSCEAR reports [21,22]. Davis et al. [23] proposed a model that accounts for the absence of a risk decline at higher radiation doses. Dasu et al. [24] added the effect of dose fractionation. Timlin et al. [25], Sachs and Brenner [26], and Shuryak et al. [27,28] proposed

other models that consider more complex biological processes. Among these, the Schneider mechanistic model [5,6], which is adopted in this work, offers the advantage of accounting for both the fractionation schedule and cell proliferation occurring between RT fractions.

The aim of this study is to retrospectively estimate long-term lung cancer induction risk for SF and HF 3D Conformal Radiotherapy (3D-CRT) in breast cancer. We also evaluated the feasibility of estimating these risks a priori and integrating them into the treatment planning workflow. To support this evaluation, we implemented a script within the Eclipse™ environment. The script provides rapid, in-planning visualization of risk estimates.

2. Materials and Methods

2.1. Patient Selection and Treatment Setup

Fifty-eight Sicilian women aged between 30 and 70 years with early-stage BC were included in this study. The mean patient age was 55 years, with a standard deviation of 10 years. These women were treated at Humanitas-Istituto Clinico Catanese (H-ICC) (Misterbianco, Italy) between 2015 and 2021. All data were fully anonymized and cannot be traced back to individuals. RT was delivered using a tangential field technique, encompassing the chest wall and a small portion of the ipsilateral lung within the irradiated volume. An anterior field with an angled gantry was used to avoid the spinal cord, esophagus, and contralateral breast. Treatment plans were calculated using the Analytical Anisotropic Algorithm (AAA, version 15.6.06) within the Eclipse v. 16.1 Treatment Planning System (TPS) by Varian Medical Systems (Palo Alto, CA, version 15.6.8, https://www.varian.com/), based on CT scans with 2.5 mm slice thickness. Therapy was performed using a Varian TrueBeam 2.7 linear accelerator (https://www.varian.com/), which produces 6 MV photon beams with two opposite tangential static field techniques. For all treatment plans, the maximum dose (always within the PTV) was lower than 110% and at least 95% of the prescribed dose covered 95% of the PTV volume. OAR dose constraints, converted to equivalent dose, were respected: V5 < 40%; V20 < 20%; D_{mean} < 7 Gy [29–33]. Treatment plans were rescaled to an HF schedule using the same irradiation geometry—including field sizes, beam angles, and beam arrangements—to assess differences in ipsilateral lung carcinogenesis risk, and all OAR dose constraints were respected.

2.2. Risk Estimation

The Schneider mechanistic model [5,6] integrates the LNT framework derived from atomic bomb survivor data with cancer incidence data from a cohort of patients with Hodgkin's disease treated with RT. It provides site-specific dose–response relationships for solid cancers induced by therapeutic radiation exposures [6]. It is based on the Organ Equivalent Dose (***OAR***):

$$\boldsymbol{OED} = \frac{\mathbf{1}}{\boldsymbol{V_T}} \sum_i \boldsymbol{RED}(\boldsymbol{D_i}) \boldsymbol{V}(\boldsymbol{D_i}), \quad (1)$$

This quantity represents, for any inhomogeneous dose distribution in an organ, the dose in Gray, which, when distributed uniformly, causes the same radiation-induced cancer incidence [34]. When the dose–response relationship is linear, cancer risk is proportional to the average organ dose. However, at higher dose levels, the ***OED*** is used instead of the average dose to more accurately quantify the risk of radiation-induced cancer [6]. The Risk Equivalent Dose (***RED***) represents the dose–response relationship for radiation-induced cancer, expressed in units of dose:

$$\boldsymbol{RED}(\boldsymbol{D}) = \frac{\boldsymbol{e}^{\boldsymbol{\alpha' D}}}{\boldsymbol{\alpha' R}} \left(\mathbf{1} - \mathbf{2}\boldsymbol{R} + \boldsymbol{R}^{\mathbf{2}} \boldsymbol{e}^{\boldsymbol{\alpha' D}} - (\mathbf{1} - \boldsymbol{R})^{\mathbf{2}} \boldsymbol{e}^{-\frac{\boldsymbol{\alpha' R}}{\mathbf{1}-\boldsymbol{R}} \boldsymbol{D}} \right), \quad (2)$$

where D is the total dose (50 Gy and 42.56 Gy for SF and HF BC treatments, respectively) and R is the repopulation parameter, which characterizes the tissue repopulation/repair ability between two dose fractions. The R-value ranges from 0 to 1, where tissues with no capacity for repopulation or repair correspond to R = 0, and tissues capable of full repair or repopulation correspond to R = 1. The number of cells killed during irradiation is proportional to α', i.e., the kill parameter for fractionated treatments, which is defined as follows:

$$\alpha' = \alpha + \beta d_f, \tag{3}$$

where α and β are linear-quadratic model parameters specific to the irradiated tissue, and d_f is the dose per fraction. α, α/β, and R values were determined based on epidemiological studies of patients with HD treated with radiation therapy. This is because calculating the OED requires 3D dose distribution data, which is generally not available in epidemiological studies on RT-induced secondary cancers. However, for HD patients, this information can be reconstructed. For example, Travis et al. [10] studied lung cancer induction for mantle field treatments of HD, reconstructing the point doses where the secondary cancer was located. This capability to reconstruct dose distributions is one of the reasons why HD data were selected for model development. Additionally, HD patients are generally treated at a relatively young age with curative intent, allowing secondary cancer incidence rates for various organs to be determined with good precision [6]. Another advantage is that treatment techniques for HD have remained largely consistent over the past 30 years, with little variation between institutions. These factors enable the reconstruction of a statistically averaged OED representative of a large cohort of HD patients. The Excess Absolute Risk (EAR) for the development of secondary cancer after RT, referring to the entire organ, is defined as follows:

$$EAR = \frac{1}{V_T}\sum_i V(D_i)\beta_0 RED(D_i)\mu(age_e, age_a), \tag{4}$$

where V_T is the total organ volume, $V(D_i)$ is the volume of the ipsilateral lung absorbing a dose of D_i, and β_0 is the mutation parameter (initial slope of the LNT model). μ is the modifying function; it introduces carcinogenesis risk age dependence:

$$\mu(age_e, age_a) = exp(\gamma_e(age_e - 30) + \gamma_a ln\left(\frac{age_a}{70}\right)), \tag{5}$$

where γ_e and γ_a are two organ-specific parameters derived from the LSS study [3], age_e is the age of the patient during exposure, and age_a is the attained patient's age. Based on published data, the parameters of the mechanistic model employed for lung cancer risk assessments were α (Gy^{-1}) = 0.061, α/β = 3, R = 0.84, β_0 (10^4 PY $Gy)^{-1}$ = 8.0 (5.5; 11), γ_e (Y^{-1}) = 0.002, γ_a (Y^{-1}) = 4.23 [6–11].

Schneider's model concludes with the calculation of the Excess Absolute Risk (EAR); however, it can be extended further to derive two additional risk metrics: the Lifetime Attributable Risk (LAR) and the Relative Risk (RR), as conducted by Mazonakis et al. [35]. These metrics account not only for the radiation-induced risk but also incorporate the patient's survival probability and the baseline (intrinsic) risk of developing the disease independently of RT. By weighting the EAR with the patient's survival probability between the exposure age (age_e) and attained age (age_a), the LAR for developing secondary malignancies can be determined as follows:

$$LAR = \sum_{age_e+L}^{75} EAR(OED, age_e, age_a)\frac{S(age_a)}{S(age_e)}, \tag{6}$$

where $S(age_a)/S(age_e)$ represents the regional survival probability, as provided by ISTAT (Istituto Nazionale di Statistica), for a healthy individual living in Sicily (Italy) to survive from age_e to age_a [36]. L is a free cancer risk interval or latency period (5 years for BC) [37]. The probability of survival to age L, defined as $S(age_e + 5)/S(age_e)$, was calculated using internal H-ICC statistics from a cohort of 915 patients. The resulting survival probability is 98.60% for individuals younger than 65 years at exposure, and 96.34% for all other cases. In this study, the expected age was fixed at 75 years, based on the following considerations: (i) the Schneider model is derived from A-bomb survivor data, which assume an average age at exposure of 30 years and an expected age of 70 years; (ii) statistically robust data on the Lifetime Intrinsic Risk (***LIR***) of developing malignancies, provided by ISTAT, are available up to age 75. Beyond this age, a marked decline in the year-to-year survival probability (from age_i to age_{i+1}) is observed (Figure 1), which compromises the reliability of ***LIR*** estimates. Independent of the RT treatment, for each person, there is a certain organ-, gender-, and age-dependent ***LIR*** for developing a malignancy in the radiosensitive structure of interest. In this study, ***LIR*** values were obtained using lung cancer incidence data for Sicilian women resident in Catania provided by the Integrated Cancer Registry CT-ME-EN (AOU Policlinico "G. Rodolico—San Marco", Catania, Italy). ***LIR*** values are equal to 5.37%, 5.34%, 5.26%, 5.10%, 4.70%, 3.99%, 3.18%, 2.16%, and 1.17% or exposure ages ranging from 30 to 70 years in 5-year increments. ***LAR*** values, obtained using the Schneider model, can be compared with the ***LIR*** through the patient-specific Relative Risk (***RR***) calculation (Equation (7)), which quantifies the increase in baseline cancer probability for an irradiated individual compared to an unexposed one. This metric enables an evaluation of which fractionation scheme (SF or HF) is associated with a higher risk of radiation-induced cancer.

$$RR = \frac{LAR + LIR}{LIR}, \tag{7}$$

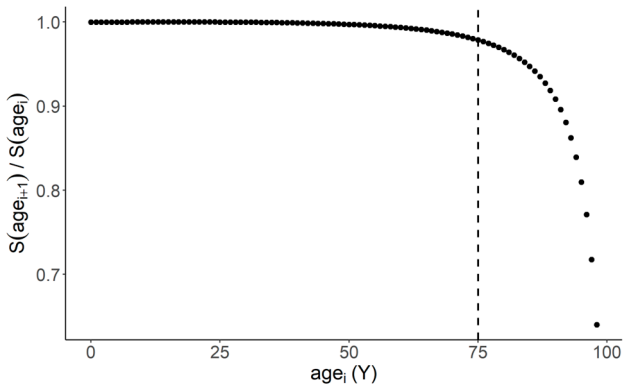

Figure 1. Probability $S(age_{i+1})/S(age_i)$ of a healthy individual surviving from age_i to age_{i+1}, based on regional survival data from ISTAT (Istituto Nazionale di Statistica) for Sicily, Italy [36].

2.3. Script Implementation

To compute the risk-related metrics defined by the Schneider mechanistic model (***OED***, ***EAR***, and ***LAR***), an in-house plug-in script was developed using the Eclipse Scripting Application Programming Interface (ESAPI). The script was implemented in C#, the programming language required by the platform. It can be launched directly from the Eclipse™ user interface, enabling access to the data of the currently open patient. Specifically, the context of the running Eclipse™ instance is passed to the script as an input parameter [38], which includes treatment plan data and CT images active in Eclipse™. This direct access allows the script to retrieve the treatment plan information necessary for risk calculations, such as the i-th volume ($V(D_i)$) and i-th dose (D_i) from the OAR differential Dose–Volume Histogram (DVH) (Equation (2)), as well as the patient's age at exposure

(age_e). Population-specific parameters, including L and $S(age_a)/S(age_e)$, are predefined within the script.

Upon execution for a given treatment, the Organ At Risk (***OAR***) of interest (e.g., lungs) can be selected via a scrolling window from the list of previously contoured structures. Following this selection, all calculations defined by Schneider's model are performed automatically. The output includes structure volume (cm^3), Organ Equivalent Dose (***OED***, Gy), Excess Absolute Risk (***EAR***, per 10,000 person-years), and Lifetime Attributable Risk (***LAR***, per 10,000 persons). Additionally, patient, ***OAR***, and risk information are simultaneously saved to an external .txt file, facilitating the creation of a database for subsequent statistical risk analyses. The script workflow is illustrated in Figure 2.

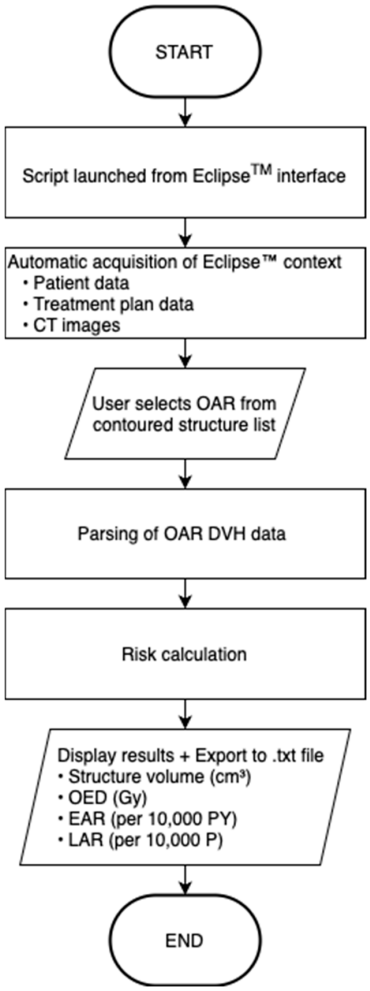

Figure 2. Eclipse™ plug-in script workflow.

3. Results

Figures 3–5 show the density plots (a) and boxplots (b) of ***OED***, ***EAR***, and ***LAR*** for both treatment schemes. Table 1 reports the minimum, maximum, and mean values for each of these metrics. Since treatment plans were recalculated by altering only the fractionation schedule (SF vs. HF), the observed risk variations for the same patient are primarily attributable to changes in total dose (***D***) and dose per fraction (d_f). The ***OED*** distribution shows a rightward shift for the 3D-CRT SF treatment compared to HF (Figure 3). As ***OED*** directly influences ***EAR*** and ***LAR*** (Equations (4) and (6)), similar trends are observed in Figures 4 and 5.

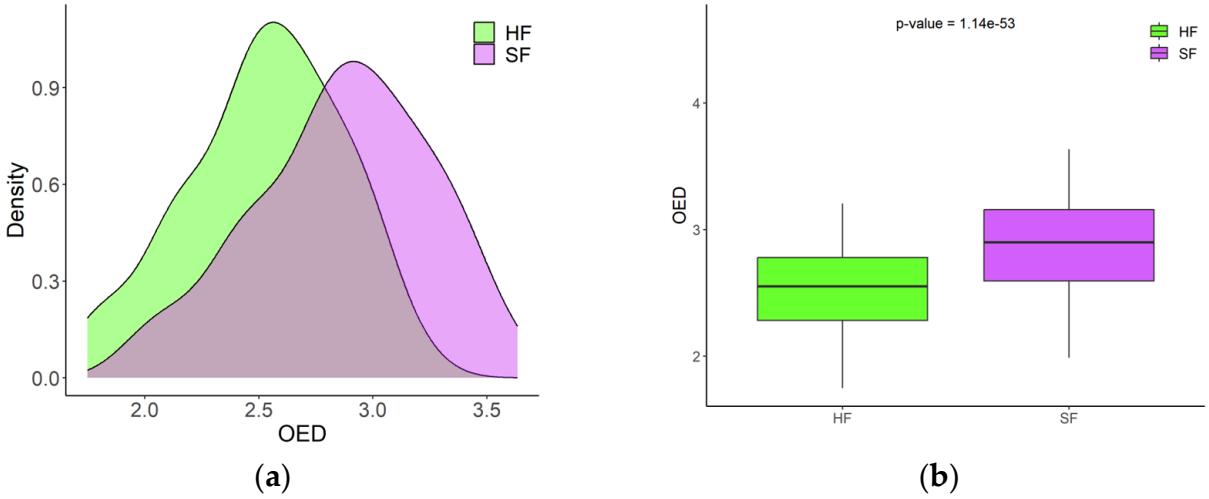

Figure 3. Organ Equivalent Dose (***OED***, in Gy) for 3D conformal radiotherapy (3D-CRT) treatment plans using standard fractionation (SF) and hypofractionation (HF). (**a**) Density curves illustrate the distribution of ***OED*** values for patients in each fractionation group. (**b**) Boxplots show group medians (center line), interquartile ranges (boxes), and data spread (whiskers). The reported *p*-value from a one-tailed paired Student's *t*-test compares SF and HF groups.

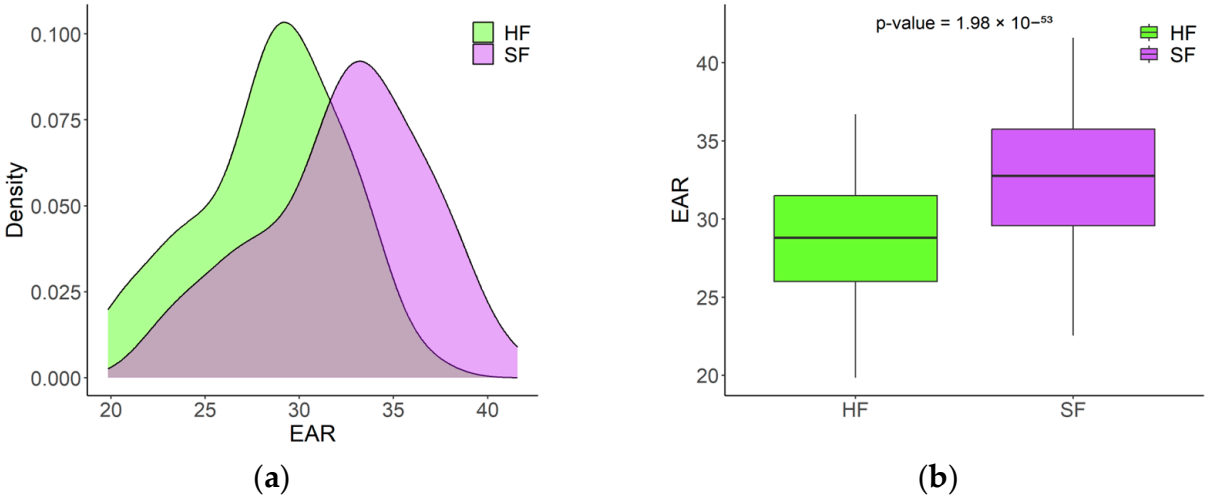

Figure 4. Excess Absolute Risk (***EAR***) for 3D conformal radiotherapy (3D-CRT) treatment plans using standard fractionation (SF) and hypofractionation (HF). (**a**) Density curves illustrate the distribution of ***EAR*** values for patients in each fractionation group. (**b**) Boxplots show group medians (center line), interquartile ranges (boxes), and data spread (whiskers). The reported *p*-value from a one-tailed paired Student's *t*-test compares SF and HF groups.

To assess whether one treatment approach results in a significantly higher risk of radiation-induced lung cancer, a one-tailed paired Student's *t*-test was performed on ***OED***, ***EAR***, and ***LAR*** values for SF and HF plans. The test assumed that paired differences are normally distributed, the data are continuous, each pair is dependent, and the pairs are mutually independent. The results indicate that the two datasets belong to distinct populations (p-value < 0.01), due to a consistent increase in ***OED*** for SF compared to HF (mean ***OED*** ratio = 1.137 $\pm$ 0.002). ***LAR*** depends on ***OED*** and the time interval between age_e and age_a, weighted by survival probability.

Figure 6 illustrates the variation in ***LAR*** between SF and HF as a function of age_e. For the same patient, ***LAR*** is systematically lower with HF due to the reduced ***OED*** associated with its lower prescription dose. The figure also highlights the inverse correlation between

LAR and ***age$_e$***: younger patients face a higher risk, given their longer life expectancy and greater time window for secondary cancer development. Data dispersion reflects inter-patient variability in ***OAR*** morphology, which affects ***LAR*** computation.

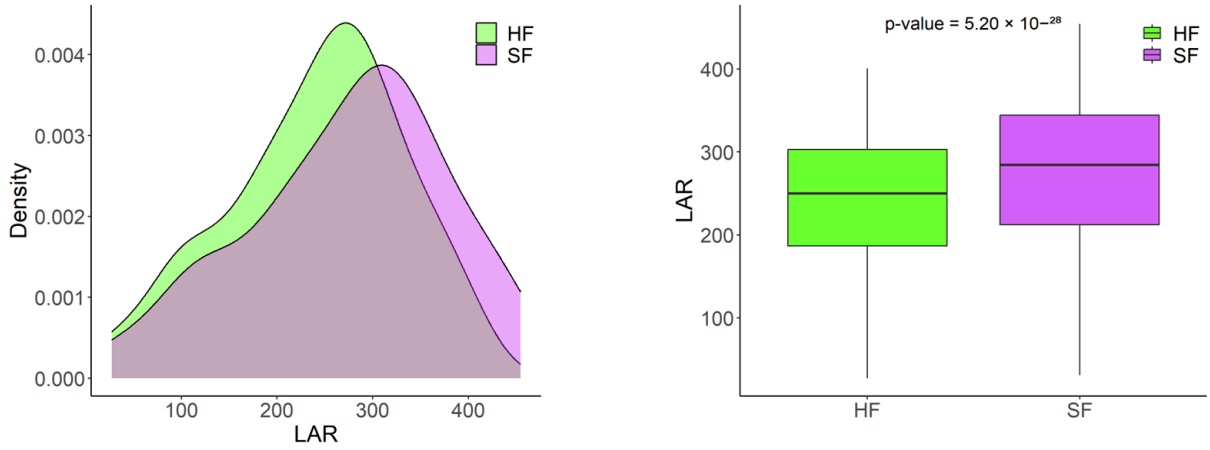

(**a**) (**b**)

Figure 5. Standard fractionation (SF) and hypofractionation (HF). (**a**) Density curves illustrate the distribution of ***LAR*** values for patients in each fractionation group. (**b**) Boxplots show group medians (center line), interquartile ranges (boxes), and data spread (whiskers). The reported *p*-value from a one-tailed paired Student's *t*-test compares SF and HF groups.

Table 1. V_5, V_{20}, Organ Equivalent Dose (***OED***), Excess Absolute Risk (***EAR***), Lifetime Attributable Risk (***LAR***), and Relative Risk (***RR***) for 3D-CRT standard fractionated (SF) and hypofractionation (HF) approaches.

Treatment Type	V5 (%)	V20 (%)	OED (Gy)	EAR (1/10,000 PY)	LAR (1/10,000 P)	Treatment Type
3D-CRT SF	24.7 (12.3–35.3)	11.3 (2.1–19.2)	2.9 (2.0–3.6)	32 (23–42)	274 (31–455)	1.80 (1.26–1.86)
3D-CRT HF	22.0 (9.4–32.1)	11.3 (1.9–17.9)	2.5 (1.7–3.2)	28 (20–37)	241 (27–400)	1.70 (1.23–1.76)

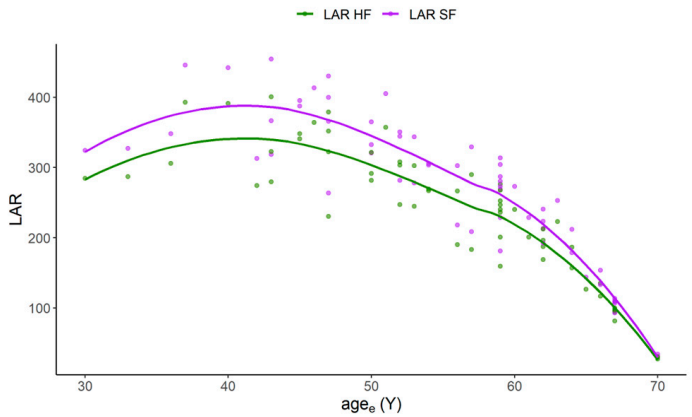

Figure 6. Attributable lifetime risk (***LAR***) as a function of age at exposure for 3D conformal radiotherapy (3D-CRT) treatment plans with standard fractionation (SF) and hypofractionation (HF). Curves represent trends for each fractionation plan; points indicate patient-specific values.

Finally, ***RR*** values were calculated for each patient using age- and region-specific ***LIR*** data for lung cancer in Sicilian women. The ***RR*** ranged from 1.26 to 1.86 (mean value 1.80) for SF, and from 1.23 to 1.76 (mean value 1.70) for HF.

4. Discussion

BC RT treatments are typically delivered using two different fractionation schedules: SF and HF. Clinical trial results report 10-year local recurrence rates of 4.3% for HF and 5.5% for SF [39]. For this reason, HF is the preferred approach, although SF is still used in specific clinical conditions.

In this study, the difference in RT-induced lung cancer risk for BC was evaluated for both fractionation schemes using Schneider's model. The risk was estimated for 58 Sicilian women aged between 30 and 70 years, all treated with a 3D-CRT SF approach between 2015 and 2021. Risk factor calculations were performed using a custom-developed Eclipse™ script. This tool enables immediate visualization of relevant risk metrics. It significantly reduces the time compared to the standard workflow of exporting the DVH file and applying Schneider's model post hoc. The results obtained in this work, alongside those from the literature, are reported in Tables 1 and 2, respectively. For the SF approach, ***EAR*** values ranged from 23 to 42 (per 10,000 PY) and ***LAR*** values from 31 to 455 (per 10,000 P). For the HF approach, ***EAR*** values ranged from 20 to 37 (per 10,000 PY) and LAR values from 27 to 400 (per 10,000 P).

Table 2. Excess Absolute Risk (EAR) and Lifetime Attributable Risk (LAR) values for lung carcinogenesis risk after RT treatment [35,40].

Paper	Prescription Dose	Treatment Type	EAR (1/10,000 PY)	LAR (1/10,000 P)	age_a (Y)
Mazonakis et al. [35]	50 Gy at 2 Gy/fraction	IMRT	/	359–494	75
Mazonakis et al. [35]	42.56 Gy at 2.66 Gy/fraction	IMRT	/	316–437	75
Paganetti et al. [40]	50 Gy at 2 Gy/fraction or 50.4 Gy at 1.8 Gy/fraction	3D-CRT	46 (23–55)	458 (275–654)	70
Paganetti et al. [40]	50 Gy at 2 Gy/fraction or 50.4 Gy at 1.8 Gy/fraction	VMAT	61 (58–64)	656 (410–770)	70

Mazonakis et al. [35] reported ***LAR*** values ranging from 359 to 494 (1/10,000 P) for the Intensity-Modulated Radiation Therapy (IMRT) SF approach, and from 316 to 437 (1/10,000 P) for the IMRT HF approach. Paganetti et al. [40] found ***EAR*** values between 23 and 55 (1/10,000 PY) and ***LAR*** values between 275 and 654 (1/10,000 P) for 3D-CRT SF. For Volumetric Modulated Arc Therapy (VMAT), they reported ***EAR*** values between 58 and 64 and ***LAR*** values between 410 and 770. These studies commonly applied Schneider's model for risk assessment but differ in terms of treatment technique and, in some cases, prescription dose. Only one of them, i.e., Paganetti et al. [40], evaluated RT-induced lung cancer risk for 3D-CRT SF in breast cancer patients, with prescription doses of either 50 Gy in 25 fractions of 2.0 Gy or 50.4 Gy in 28 fractions of 1.8 Gy. The smaller patient sample analyzed by Paganetti et al. (n = 10) may partly explain the narrower range of results compared to our study, which included a larger cohort of 58 patients. Any comparison with the findings of Paganetti et al. should consider these differences, as well as the fact that they assumed an age_a of 70 years.

For the same ***OAR***, the risk of radiation-induced cancer also depends on the treatment technique employed. For instance, IMRT typically results in higher doses to the contralateral breast compared to 3D-CRT. Mazonakis et al. [38] extended their analysis to this ***OAR***, reporting ***OED*** values of up to 0.99 Gy for SF and 0.86 Gy for HF. The corresponding patient-specific ***RR*** ranged from 1.04 to 1.10 for SF, and from 1.03 to 1.09 for HF. Paganetti et al. [40] conducted a study comparing multiple RT techniques—3D-CRT, VMAT, and Pencil Beam

Scanning (PBS). Their results indicated that 3D-CRT yielded the lowest estimated risks for secondary thyroid and esophageal cancers, while PBS offered advantages in reducing risks to the lung and contralateral breast. Conversely, VMAT was associated with the highest overall secondary cancer risks. In our analysis, a paired *t*-test (p-value < 0.01) comparing ***LAR*** values between SF and HF schedules showed that HF is associated with a statistically significant reduction in RT-induced lung cancer risk. This reduction is due to the lower exposure of the ipsilateral lung to low-dose regions in HF treatments. Because RED depends exponentially on both total dose (***D***) and dose per fraction (d_f), the reduced lung dose translates into a meaningful decrease in carcinogenic risk with the HF regimen.

In this study, the use of SF 3D-CRT was estimated to result in a ***LIR*** increase of 26–86%, while HF treatment may lead to an increase of 23–76%. The corresponding ***RR*** values, derived from ***EAR*** estimates using the Schneider model, are comparable to those reported in the meta-analysis of 762,468 patients conducted by Grantzau et al. [15] on the risk of second non-breast cancers following RT for BC. They reported RR values of 1.39 (95% CI: 1.28–1.51). Using the Schneider model, Mazonakis et al. [35] reported a LIR increase of 60–81% for the SF approach and 53–73% for the HF approach. The uncertainty in the risk estimates arises from several factors [41], each potentially introducing significant variability. These include tissue modeling, the repopulation process linked to the prescribed dose, the biological mechanisms leading to tumor cell formation, the parameters of dose–response curves, and dosimetric considerations. Dores et al. [7], through independent fits to observed ***EAR*** variations, reported a Relative Standard Deviation (RSD) of 1.31 for α and 0.06 for R, while [6] found an RSD of 0.19. From a dosimetric perspective, since the ***OED*** is derived from the differential DVH, uncertainties are associated with the correspondence between the calculated and the delivered dose at specific points within the organ, particularly in regions with steep dose gradients or significant tissue inhomogeneity. The integral dose only approximates the risk to an individual organ. This is due to the non-linear dose–response relationship, meaning that the risk depends on the full 3D dose distribution rather than being directly proportional to the integral dose [42]. Another important aspect is the repeatability of the dose–volume association for organs at risk across treatment sessions. The implementation of patient immobilization systems, verification tools such as Cone Beam Computed Tomography (CBCT), Electronic Portal Imaging Devices (EPID), and Surface-Guided Radiation Therapy (SGRT) systems integrated with the LINAC has significantly reduced this source of uncertainty. However, clinical data remain limited for establishing epidemiological studies that fully account for these factors. Under these conditions, hybrid approaches combining mechanistic and empirical methods appear promising for risk model development. This is particularly true when incorporating factors known to influence the risk of second cancers following RT [4].

EAR, ***LAR***, and ***RR*** estimations require statistical data that must be representative of the study population to avoid overestimating or underestimating the risk. For this reason, a preliminary research phase was conducted to identify statistics specific to the Sicilian female population. In our view, this step is essential to enhance the reliability of the obtained results. When patients are treated with ionizing radiation, a stochastic risk of carcinogenesis is introduced. Our results show that, according to the RT-induced lung cancer risk model, the estimated risk for breast cancer patients is lower for 3D-CRT HF treatments compared to SF treatments. In this context, the use of customized scripts that interface with treatment planning systems such as Eclipse™ represents a valuable tool. These scripts can support clinicians by providing real-time risk estimates during the planning phase, thus facilitating the integration of risk-based considerations into routine clinical workflows.

This study has some limitations. While the Schneider model provides valuable probabilistic risk indicators, it does not yield definitive clinical predictions. Therefore, these risk estimates should be interpreted with caution and integrated into clinical decision-making alongside patient-specific factors and clinical judgment. Additionally, the sample size is relatively small (n = 18), and data were collected from a single institution. Nonetheless, the primary objective was to compare fractionation patterns with respect to induced cancer risk, and this was achieved. The main result is that ***OED*** increases with standard fractionation, and this relies on the underlying physical dose distribution and organ-at-risk considerations, which are largely independent of region- or institution-specific factors that primarily influence ***LAR*** and ***RR***. These points support the model's applicability, despite design limitations.

5. Conclusions

This study showed that the estimated risk of radiation-induced lung cancer in breast cancer patients treated with 3D-CRT is significantly lower for hypofractionated (HF) schedules compared to standard fractionation (SF). These findings align with existing literature and support the increasing preference for HF approaches in clinical practice. The integration of Schneider's model into the treatment planning process proved effective in enabling real-time risk estimation during plan development. Incorporating such tools into clinical workflows may lead to more informed and proactive risk management. The absolute risk reductions observed could translate into a lower incidence of lung cancer at the population level, highlighting their relevance for clinical decision-making. Finally, the use of demographic data specific to the Sicilian female population strengthens both the reliability and the contextual validity of the results.

Author Contributions: Conceptualization, A.D., G.S., and C.M.; methodology, A.D., G.S. and C.M.; software, A.D., M.P., L.Z. and G.R.B.; validation, G.S., C.M. and A.M.G.; formal analysis, A.D. and G.S.; investigation, A.D. and G.S.; resources, C.M. and A.G.; data curation, A.D., G.S., E.B., N.C. and C.M.; writing—original draft preparation, A.D. and G.S.; writing—review and editing, A.D., G.S. and A.M.G.; visualization, G.S.; supervision, G.S., C.M. and A.M.G.; project administration, G.S., C.M. and A.G.; funding acquisition, G.S. and C.M. All authors have read and agreed to the published version of the manuscript.

Funding: This research received no external funding.

Institutional Review Board Statement: Not applicable.

Informed Consent Statement: Not applicable.

Data Availability Statement: The original contributions presented in the study are included in the article. Further inquiries can be directed to the corresponding author.

Acknowledgments: This research is part of the project APE supported by "Piano di incentivi per la ricerca di Ateneo 2020/2022 (Pia.ce.ri)"—Linea di Intervento 3—STARTING GRANT of the University of Catania.

Conflicts of Interest: The authors declare no conflicts of interest.

References

1. McGale, P.; Correa, C.; Cutter, D.; Duane, F.; Ewertz, M.; Gray, R.; Mannu, G.; Peto, R.; Whelan, T.; Darby, S.; et al. Effect of Radiotherapy after Mastectomy and Axillary Surgery on 10-Year Recurrence and 20-Year Breast Cancer Mortality: Meta-Analysis of Individual Patient Data for 8135 Women in 22 Randomised Trials. *Lancet* **2014**, *383*, 2127–2135. [CrossRef]
2. Allemani, C.; Weir, H.K.; Carreira, H.; Harewood, R.; Spika, D.; Wang, X.-S.; Bannon, F.; Ahn, J.V.; Johnson, C.J.; Bonaventure, A.; et al. Global Surveillance of Cancer Survival 1995–2009: Analysis of Individual Data for 25 676 887 Patients from 279 Population-Based Registries in 67 Countries (CONCORD-2). *Lancet* **2015**, *385*, 977–1010. [CrossRef]

3. Preston, D.L.; Ron, E.; Tokuoka, S.; Funamoto, S.; Nishi, N.; Soda, M.; Mabuchi, K.; Kodama, K. Solid Cancer Incidence in Atomic Bomb Survivors: 1958–1998. *Radiat. Res.* **2007**, *168*, 1–64. [CrossRef]
4. Dasu, A.; Toma-Dasu, I. Models for the Risk of Secondary Cancers from Radiation Therapy. *Phys. Medica* **2017**, *42*, 232–238. [CrossRef] [PubMed]
5. Schneider, U. Mechanistic Model of Radiation-induced Cancer after Fractionated Radiotherapy Using the Linear-quadratic Formula. *Med. Phys.* **2009**, *36*, 1138–1143. [CrossRef] [PubMed]
6. Schneider, U.; Sumila, M.; Robotka, J. Site-Specific Dose-Response Relationships for Cancer Induction from the Combined Japanese A-Bomb and Hodgkin Cohorts for Doses Relevant to Radiotherapy. *Theor. Biol. Med. Model.* **2011**, *8*, 27. [CrossRef]
7. Dores, G.M.; Metayer, C.; Curtis, R.E.; Lynch, C.F.; Clarke, E.A.; Glimelius, B.; Storm, H.; Pukkala, E.; van Leeuwen, F.E.; Holowaty, E.J.; et al. Second Malignant Neoplasms Among Long-Term Survivors of Hodgkin's Disease: A Population-Based Evaluation Over 25 Years. *J. Clin. Oncol.* **2002**, *20*, 3484–3494. [CrossRef] [PubMed]
8. Schneider, U.; Stipper, A.; Besserer, J. Dose-Response Relationship for Lung Cancer Induction at Radiotherapy Dose. *Z Med. Phys.* **2010**, *20*, 206–214. [CrossRef]
9. Schneider, U.; Sumila, M.; Robotka, J.; Gruber, G.; Mack, A.; Besserer, J. Dose-Response Relationship for Breast Cancer Induction at Radiotherapy Dose. *Radiat. Oncol.* **2011**, *6*, 67. [CrossRef]
10. Travis, L.B. Lung Cancer Following Chemotherapy and Radiotherapy for Hodgkin's Disease. *CancerSpectrum Knowl. Environ.* **2002**, *94*, 182–192. [CrossRef]
11. Travis, L.B.; Hill, D.A.; Dores, G.M.; Gospodarowicz, M.; van Leeuwen, F.E.; Holowaty, E.; Glimelius, B.; Andersson, M.; Wiklund, T.; Lynch, C.F.; et al. Breast Cancer Following Radiotherapy and Chemotherapy Among Young Women with Hodgkin Disease. *JAMA* **2003**, *290*, 465. [CrossRef]
12. Koulis, T.; Phan, T.; Olivotto, I. Hypofractionated Whole Breast Radiotherapy: Current Perspectives. *Breast Cancer Targets Ther.* **2015**, *7*, 363–370. [CrossRef] [PubMed]
13. Hall, E.J.; Wuu, C.-S. Radiation-Induced Second Cancers: The Impact of 3D-CRT and IMRT. *Int. J. Radiat. Oncol. Biol. Phys.* **2003**, *56*, 83–88. [CrossRef] [PubMed]
14. Grantzau, T.; Thomsen, M.S.; Væth, M.; Overgaard, J. Risk of Second Primary Lung Cancer in Women after Radiotherapy for Breast Cancer. *Radiother. Oncol.* **2014**, *111*, 366–373. [CrossRef]
15. Grantzau, T.; Overgaard, J. Risk of Second Non-Breast Cancer after Radiotherapy for Breast Cancer: A Systematic Review and Meta-Analysis of 762,468 Patients. *Radiother. Oncol.* **2015**, *114*, 56–65. [CrossRef]
16. Grantzau, T.; Overgaard, J. Risk of Second Non-Breast Cancer among Patients Treated with and without Postoperative Radiotherapy for Primary Breast Cancer: A Systematic Review and Meta-Analysis of Population-Based Studies Including 522,739 Patients. *Radiother. Oncol.* **2016**, *121*, 402–413. [CrossRef] [PubMed]
17. Henson, K.E.; McGale, P.; Taylor, C.; Darby, S.C. Radiation-Related Mortality from Heart Disease and Lung Cancer More than 20 Years after Radiotherapy for Breast Cancer. *Br. J. Cancer* **2013**, *108*, 179–182. [CrossRef]
18. Mazonakis, M.; Damilakis, J. Out-of-Field Organ Doses and Associated Risk of Cancer Development Following Radiation Therapy with Photons. *Phys. Medica* **2021**, *90*, 73–82. [CrossRef]
19. Taylor, C.; Correa, C.; Duane, F.K.; Aznar, M.C.; Anderson, S.J.; Bergh, J.; Dodwell, D.; Ewertz, M.; Gray, R.; Jagsi, R.; et al. Estimating the Risks of Breast Cancer Radiotherapy: Evidence from Modern Radiation Doses to the Lungs and Heart and From Previous Randomized Trials. *J. Clin. Oncol.* **2017**, *35*, 1641–1649. [CrossRef]
20. Gray, L.H. Cellular Radiation Biology Symposium Considering Radiation Effects in the Cell and Possible Implications for Cancer Therapy. *Postgrad Med. J.* **1966**, *42*, 795. [CrossRef]
21. United Nations. *Scientific Committee on the Effects of Atomic Radiation, Issuing Body. Sources and Effects of Ionizing Radiation: UNSCEAR 1996 Report to the General Assembly, with Scientific Annex*; United Nations: New York, NY, USA, 1996.
22. United Nations Scientific Committee on the Effects of Atomic Radiation Sources and Effects of Ionizing Radiation. *Unscear 2000 Report to the General Assembly, with Scientific Annexes*; United Nations: New York, NY, USA, 2000.
23. Davis, R.H. Production and Killing of Second Cancer Precursor Cells in Radiation Therapy: In Regard to Hall and Wuu (Int J Radiat Oncol Biol Phys 2003;56:83–88). *Int. J. Radiat. Oncol. Biol. Phys.* **2004**, *59*, 916. [CrossRef]
24. Daşu, A.; Toma-Daşu, I.; Olofsson, J.; Karlsson, M. The Use of Risk Estimation Models for the Induction of Secondary Cancers Following Radiotherapy. *Acta Oncol.* **2005**, *44*, 339–347. [CrossRef]
25. Timlin, C.; Warren, D.R.; Rowland, B.; Madkhali, A.; Loken, J.; Partridge, M.; Jones, B.; Kruse, J.; Miller, R. 3D Calculation of Radiation-induced Second Cancer Risk Including Dose and Tissue Response Heterogeneities. *Med. Phys.* **2015**, *42*, 866–876. [CrossRef] [PubMed]
26. Sachs, R.K.; Brenner, D.J. Solid Tumor Risks after High Doses of Ionizing Radiation. *Proc. Natl. Acad. Sci. USA* **2005**, *102*, 13040–13045. [CrossRef]
27. Shuryak, I.; Hahnfeldt, P.; Hlatky, L.; Sachs, R.K.; Brenner, D.J. A New View of Radiation-Induced Cancer: Integrating Short- and Long-Term Processes. Part I: Approach. *Radiat. Environ. Biophys.* **2009**, *48*, 263–274. [CrossRef]

28. Shuryak, I.; Hahnfeldt, P.; Hlatky, L.; Sachs, R.K.; Brenner, D.J. A New View of Radiation-Induced Cancer: Integrating Short- and Long-Term Processes. Part II: Second Cancer Risk Estimation. *Radiat. Environ. Biophys.* **2009**, *48*, 275–286. [CrossRef]
29. Venjakob, A.; Oertel, M.; Hering, D.A.; Moustakis, C.; Haverkamp, U.; Eich, H.T. Hybrid Volumetric Modulated Arc Therapy for Hypofractionated Radiotherapy of Breast Cancer: A Treatment Planning Study. *Strahlenther. Onkol.* **2021**, *197*, 296–307. [CrossRef]
30. Fogliata, A.; Seppälä, J.; Reggiori, G.; Lobefalo, F.; Palumbo, V.; De Rose, F.; Franceschini, D.; Scorsetti, M.; Cozzi, L. Dosimetric Trade-Offs in Breast Treatment with VMAT Technique. *Br. J. Radiol.* **2017**, *90*, 20160701. [CrossRef] [PubMed]
31. Lee, B.M.; Chang, J.S.; Kim, S.Y.; Keum, K.C.; Suh, C.-O.; Kim, Y.B. Hypofractionated Radiotherapy Dose Scheme and Application of New Techniques Are Associated to a Lower Incidence of Radiation Pneumonitis in Breast Cancer Patients. *Front. Oncol.* **2020**, *10*, 124. [CrossRef]
32. Ciabattoni, A.; Gregucci, F.; De Rose, F.; Falivene, S.; Fozza, A.; Daidone, A.; Morra, A.; Smaniotto, D.; Barbara, R.; Lozza, L.; et al. AIRO Breast Cancer Group Best Clinical Practice 2022 Update. *Tumori J.* **2022**, *108* (Suppl. 2), 1–144. [CrossRef] [PubMed]
33. Marks, L.B.; Yorke, E.D.; Jackson, A.; Ten Haken, R.K.; Constine, L.S.; Eisbruch, A.; Bentzen, S.M.; Nam, J.; Deasy, J.O. Use of Normal Tissue Complication Probability Models in the Clinic. *Int. J. Radiat. Oncol. Biol. Phys.* **2010**, *76*, S10–S19. [CrossRef] [PubMed]
34. Schneider, U.; Zwahlen, D.; Ross, D.; Kaser-Hotz, B. Estimation of Radiation-Induced Cancer from Three-Dimensional Dose Distributions: Concept of Organ Equivalent Dose. *Int. J. Radiat. Oncol. Biol. Phys.* **2005**, *61*, 1510–1515. [CrossRef]
35. Mazonakis, M.; Stratakis, J.; Lyraraki, E.; Damilakis, J. Risk of Contralateral Breast and Ipsilateral Lung Cancer Induction from Forward-Planned IMRT for Breast Carcinoma. *Phys. Medica* **2019**, *60*, 44–49. [CrossRef]
36. ISTAT. Istituto Nazionale di Statistica "Health for All–Italia". Available online: https://www.istat.it/it/archivio/14562 (accessed on 24 July 2025).
37. BEIR. *Health Risks from Exposure to Low Levels of Ionizing Radiation, BEIR-VII, Phase 2*; National Academies Press: Washington, DC, USA, 2006.
38. Varian Medical System Eclipse Scripting A. P. I. Reference Guide 2015. Available online: https://varianapis.github.io/VarianApiBook.pdf (accessed on 24 July 2025).
39. Haviland, J.S.; Owen, J.R.; Dewar, J.A.; Agrawal, R.K.; Barrett, J.; Barrett-Lee, P.J.; Dobbs, H.J.; Hopwood, P.; Lawton, P.A.; Magee, B.J.; et al. The UK Standardisation of Breast Radiotherapy (START) Trials of Radiotherapy Hypofractionation for Treatment of Early Breast Cancer: 10-Year Follow-up Results of Two Randomised Controlled Trials. *Lancet Oncol.* **2013**, *14*, 1086–1094. [CrossRef]
40. Paganetti, H.; Depauw, N.; Johnson, A.; Forman, R.B.; Lau, J.; Jimenez, R. The Risk for Developing a Secondary Cancer after Breast Radiation Therapy: Comparison of Photon and Proton Techniques. *Radiother. Oncol.* **2020**, *149*, 212–218. [CrossRef]
41. Raptis, A.; Ödén, J.; Ardenfors, O.; Flejmer, A.M.; Toma-Dasu, I.; Dasu, A. Cancer Risk after Breast Proton Therapy Considering Physiological and Radiobiological Uncertainties. *Phys. Medica* **2020**, *76*, 1–6. [CrossRef] [PubMed]
42. Timlin, C.; Loken, J.; Kruse, J.; Miller, R.; Schneider, U. Comparing Second Cancer Risk for Multiple Radiotherapy Modalities in Survivors of Hodgkin Lymphoma. *Br. J. Radiol.* **2021**, *94*, 20200354. [CrossRef] [PubMed]